Geological Survey of Canada
Open File 8929

LANDSLIDES AND DEBRIS FLOWS IN GRISE FIORD, NEAR AUSUITTUQ, NUNAVUT

ᓄᓇᐃᑦ ᑎᓲᖅᑐᑦ ᐊᒻᒪ ᓴᓂᑦ ᐃᖏᕋᓂᖕᒋᑦ ᐊᐅᓱᐃᑦᑐᒥᑦ, ᖃᓂᒋᔭᖕᒪᓂ ᐊᐅᔪᐃᑦᑐᖅ, ᓄᓇᕗᑦ

J.B.R. Eamer[1], A. Normandeau[1], P. Horton[2], T. Oppikofer[2], C. Michoud[2], D. Didier[3], A. Blais-Stevens[4]

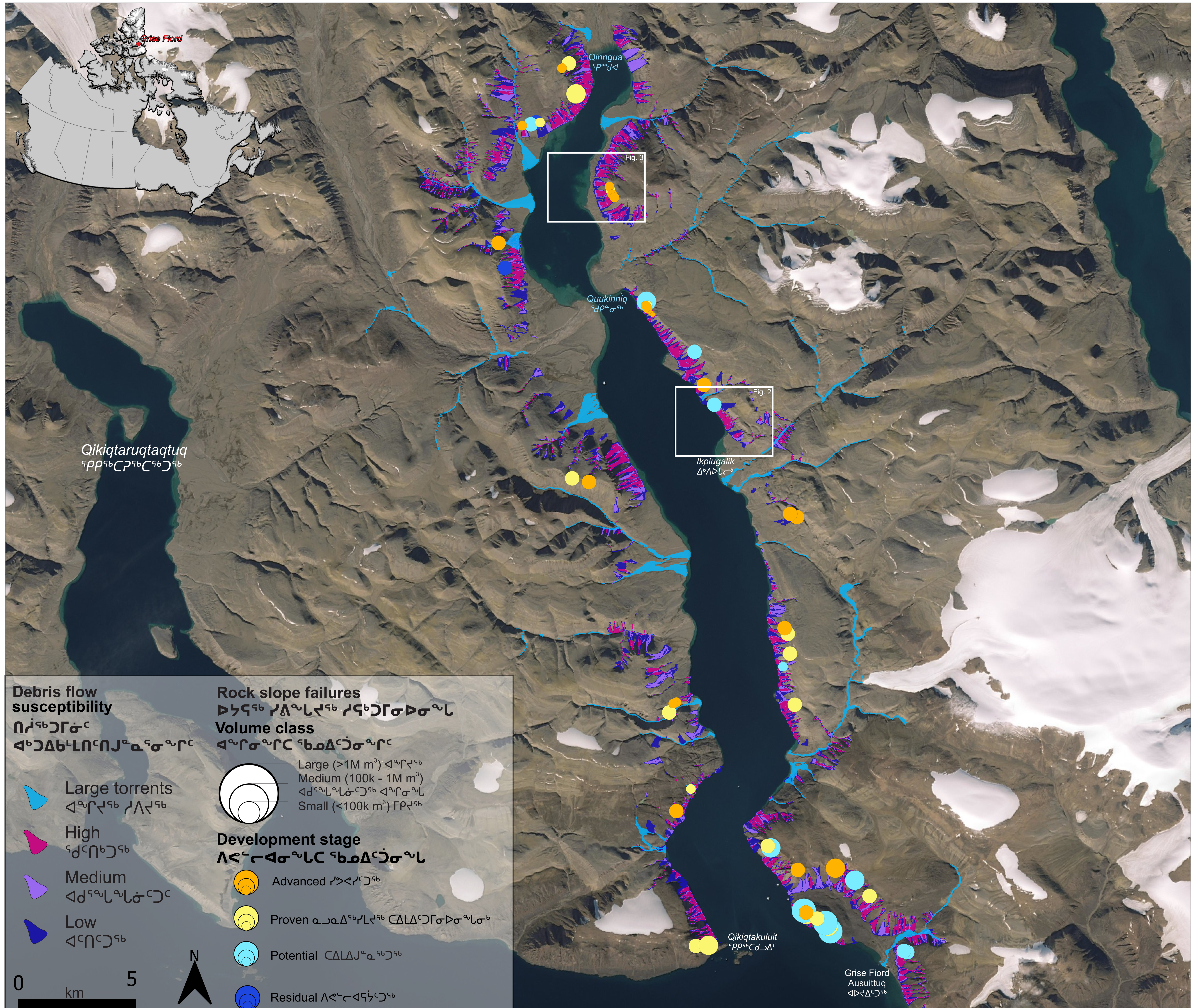

Figure 1. Debris flow susceptibility and inventory of rock slope failures in Grise Fiord.
ᐊᔾᔨᙳᐊᖅ 1. ᓴᓂᑦ ᐃᖏᕋᓂᖕᒋᑦ ᓇᕿᓪᓚᕐᓯᐊᕆᔭᐅᓴᕐᓂᖏᑦ ᐊᒻᒪ ᑎᑎᕋᖅᓯᒪᓂᖏᑦ ᐅᔭᖅᑲᐃᑦ ᓯᕗᓕᖅᑎᑦ ᑎᓲᖅᑐᑦ ᐊᐅᓱᐃᑦᑐᒥᑦ.

Acknowledgements
We are grateful to the community members of Ausuittuq for their warmth and hospitality while in the community, as well as the permission and acceptance of performing this work along their coastlines and in their waters. We especially would like to acknowledge Susie Qaunaq, Marty Kulugutuq, Jeffrey Quanaq, Terry Noah, Nolan, and Silas Pijamini.

Background

Fiords are long, flooded valleys with steep walls above the water line that are formed as glaciers that once occupied the valley retreat landwards. Because the valley walls are no longer supported by ice, they can be inherently unstable. Landslides that occur in fiords may run out into the water of the inlet, possibly resulting in tsunamis (e.g., Higman et al. 2018). Communities in eastern Nunavut are typically at or near sea-level in fiord or fiord-like environments, and as such, consideration of these risks are important (Gosse et al. 2020). Ausuittuq is located at the mouth of Grise Fiord (the inlet), southern Ellesmere Island. It is one of several north-south oriented fiords that empty into northern Jones Sound, is 45 km long, and 1 – 4 km wide. Fiord sidewalls rise to 820 m above sea level and are generally steeper up tributary river valleys. Surficial geology is dominated by colluvium, occurring as blocks and rubble. Multiple alluvial fans protrude into the fiord from seasonal river outputs and provide sources of finer sediments.

This poster follows a similar analysis performed for Pangnirtung Fiord (Normandeau et al. 2022). It describes the distribution of landslides and debris flows in Grise Fiord. The objectives of this poster are two-fold: 1) provide a preliminary assessment of the area susceptible to debris flow processes, defining potential source zones and propagation zones, and 2) map the distribution of potential rock slope failures. These preliminary results do not address the causes of slope failures or monitor movement of slope, but simply illustrate the areas that are most exposed to landslide processes. We do not provide a risk assessment, which would require a thorough monitoring of slopes.

ᓇᓗᓇᐃᔭᖅᓯᒪᓂᖏᑦ

ᑕᕐᕿᖅᑐᐃᑦ ᑕᑭᔪᑦ, ᐃᒪᕐᓯᒪᔪᑦ ᓇᖅᓴᐃᑦ, ᓯᑲᖕᒪᓪᓗᑎ ᐊᕙᓗᖕᒋᑦ ᖁᓕᒍᑦ ᐃᒪᖕᒪ ᑭᓪᓕᖕᒪ ᐊᐅᔪᑦᑐᕈᖅᓯᒪᔪᑦ ᓇᖅᓴᐅᓪᓗᑎ ᓄᓇᐅᑎᓪᓗᒍ. ᓇᖅᓴᖕᒪᓗ ᐊᕙᓗᖕᒋᑦ ᐃᑲᔪᕐᓇᐃᓕᒻᒪᕆᑦ ᓯᓚᒻᒧᑦ, ᒪᑭᑕᓗᐊᖕᒋᒍᓐᓇᖅᑐᑦ. ᓄᓇᐃᑦ ᑎᓲᖅᑕᖅᑐᑦ ᑲᖕᒋᖅᑐᓂᑦ ᐃᒪᖕᒥᓐᓃᕐᓇᖅᑐᑦ ᑲᖕᒋᖅᑐᓂᑦ, ᐃᒪᖅ ᐃᒪᖅᓱᐊᑎᑦᑎᓪᓗᓂ (ᓲᖅᓗ, Higman ᐱᓕᕆᖃᑎᖏᓪᓗ. 2018). ᓄᓇᓖᑦ ᑲᓐᓇᖕᒪᓂ ᓄᓇᕗᑦ ᖃᓂᒋᔭᖕᒪᓕᖅᑐᑦ ᐃᒪᐅᑉ ᖁᕝᕙᓯᓐᓂᖕᒪᓂ ᑲᖕᒋᖅᑐᓂ ᐅᑯᐊᓘᓂᑦ ᑲᖕᒋᖅᑑᔭᖅᑐᓂᑦ ᐊᑯᓐᓂᖕᒋᑦ, ᐊᒻᒪ ᑕᐃᒪᐃᓐᓂᖕᒪᓄᑦ, ᐃᓱᒪᒋᔭᐅᓂᖕᒋᑦ ᑖᒃᑯᐊ ᐊᑦᑕᓇᕈᑎᐅᔪᓐᓇᖅᑐᑦ ᐱᒻᒪᕆᐅᕗᖅ (ᒑᔅᓴ ᐱᓕᕆᖃᑎᖏᓗ 2020). ᐊᐅᔪᐃᑦᑐᖅ ᐃᓱᐊᓂᑦᑐᖅ ᐊᐅᓱᐃᑦᑐᖅ (ᑲᖕᒋᖅᑐᖅ), ᓂᒋᖕᒪᓗ ᐊᐅᓱᐃᑦᑐᑉ ᕿᑭᖅᑖᓗᐊ. ᐃᓚᒋᔭᐅᔪᖅ ᐊᒥᓱᓄᑦ ᐅᐊᓐᓇᒥᑦ−ᓂᒋᕐᒧᑦ ᑲᖕᒋᖅᑐᐃᑦ ᐃᒪᐃᔭᖅᑕᖅᑐᑦ ᐃᒪᖕᒪᓗ Jones Sound, 45 ᑭᓗᒦᑕᓂᑦ ᑕᑭᓂᖅᑐᖅ ᐊᒻᒪ 1 – 4 ᑭᓗᒦᑕ ᓯᓚᑐᓂᖕᒪ. ᑲᖕᒋᖅᑐᒥ ᑭᙵᖕᒋᑦ ᖁᑉᐸᑦᑐᑦ 820 ᒦᑕᐃᑦ ᖁᓛᓂ ᐃᒪᐅᑉ ᖁᕝᕙᓯᓐᓂᖕᒪᓂ ᐊᒻᒪ ᓯᕙᖕᒪᓂᖅᓴᐅᓯᔪᑦᑎ ᑰᓂᑦ, ᖄᖕᒪᓃᑦᑐᓂ ᓄᓇᖕᒪᓂ, ᓴᖅᑭᖃᑦᑕᖅᑐᑦ ᐊᖕᒋᔪᑕᐅᓪᓗᑎ ᐊᒻᒪ ᒥᑭᔪᑕᐅᓪᓗᑎ. ᐊᒥᓱᓚᐃᑦ ᑲᖕᒋᖅᑐᒨᖕᒪᔪᑦ ᐊᒥᓱᓚᓐᓂᑦ ᑰᓂᑦ ᐊᒻᒪ ᓯᐅᕋᔫᖅᑎᑎᓪᓗᑎ ᒥᑭᔪᑕᐅᓂᖅᓴᓂᑦ.

ᑖᓐᓇ ᐊᑉᓗᒥᐅᑕᖅ ᓇᓗᓇᐃᔭᐃᔪᖅ ᓇᒥᖕᒋᑦᑕᖅᓯᓂᖕᒋᑦ ᓄᓇᐃᑦ ᑎᓲᖅᑐᑦ ᐊᒻᒪ ᓴᓂᑦ ᐃᖏᕋᓂᖕᒋᑦ ᐊᐅᓱᐃᑦᑐᒥ. ᑐᕌᒐᖃᕐᓂᖓ ᐊᑉᓗᒥᐅᑕᒧᑦ ᒪᕐᕉᒃ: 1) ᐱᑕᖃᕐᑎᑦᑎᓗᓂ ᖃᐅᔨᓴᕐᓂᕐᒥᒃ ᓇᒥᓂᖕᒪ ᓴᓂᖓᓂᑦ ᐃᖏᕋᓂᖅᑐᑦ ᐱᕙᓪᓕᐊᓂᖕᒋᑦ, ᓇᓗᓇᐃᖅᑕᐅᓂᖕᒋᑦ ᓇᕿᓪᓚᕐᓯᐊᕆᔭᐅᓴᕐᓂᖕᒋᑦ ᑭᒡᒐᖕᒋᑦ, ᐊᒻᒪ 2) ᓄᓇᙳᐊᓕᐅᕐᓗᒋᑦ ᓇᒥᓂᖕᒋᑦ ᐅᔭᖅᑲᐃᑦ ᓯᕗᓕᖅᑎᑦ ᕿᓲᖅᑲᕐᓂᖅᑐᑦ. ᑖᒃᑯᐊ ᖃᐅᔨᓴᕐᓂᕐᒥᖕᓂᖅᑕᖕᒋᑦ ᐱᓇᓱᒃᑲᕐᑐᑦ ᐱᔾᔪᑎᖕᒋᕐᓂᖕᒋᑦ ᓯᕗᓕᖅᑐᓂᑦ ᑎᓲᖅᑐᓂᑦ ᐅᕙᓘᓂᑦ ᖃᐅᔨᓴᖅᓯᕐᓗᒋᑦ ᐃᖏᕋᓂᖕᒋᑦ ᓯᕗᓕᖅᑐᑦ, ᑭᓯᐊᓂᓕ ᑕᑯᓐᓇᐅᑎᑎᓗᓂ ᓇᒥᓐᓂᖕᒋᑦ ᑎᓲᖅᑕᐅᔭᖕᒍᖅᑕᖅᑐᑦ, ᐱᑕᖃᙱᑦᑐᒍᑦ ᐊᑦᑕᓇᕈᑎᐅᔪᓐᓇᖅᑐᓂᑦ ᖃᐅᔨᓴᕐᓂᖅᑐᒥᑦ, ᖃᐅᔨᓴᐃᓂᖅᑎᑦᑎᓇᓱᑦᑐᒥ ᓯᕗᓕᖅᑐᑦ.

Debris flow susceptibility

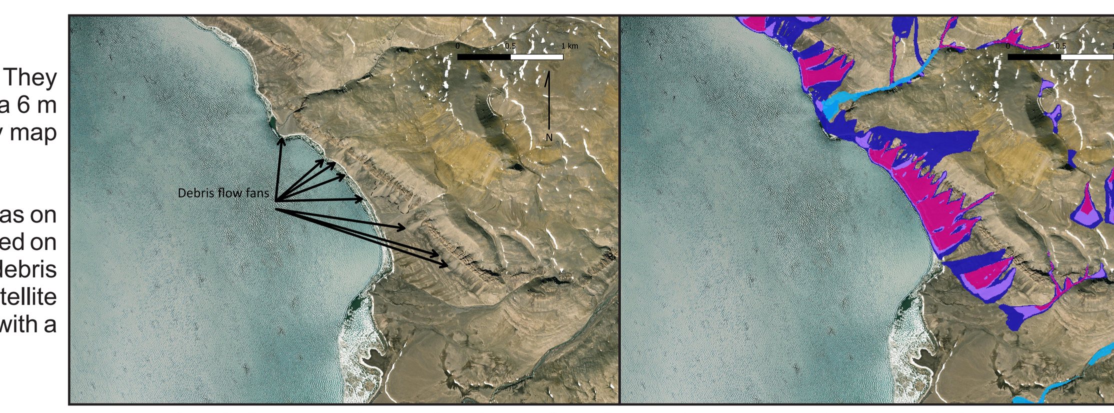

Figure 2. (left) Examples of debris flow fans in Grise Fiord, with one region of high density fans outlined by a dashed line. (right) Example of debris flow susceptibility modelling results in the same region. See Figure 1 for legend.
ᐊᔾᔨᙳᐊᖅ 2. (ᓴᐅᒥᒥ) ᐆᑦᑑᑎᒋᓗᒍ ᓴᓂᑦ ᐃᖏᕋᓂᖕᒋᑦ ᓯᐊᒻᒪᖅᓯᒪᔪᑦ ᐊᐅᓱᐃᑦᑐᒥ, ᐊᑕᐅᓯᐅᓗᓂ ᐊᖕᒋᔪᒥᑦ ᓯᐊᒻᒪᖅᐱᓯᒪᔪᖅ ᓇᓗᓇᐃᔭᖅᓯᒪᔪᑦ ᑎᑎᖅᓯᒪᔪᓂᑦ. (ᑕᓕᖅᐱᒥ) ᐆᑦᑑᑎᒋᓗᒍ ᓴᓂᑦ ᐃᖏᕋᓂᖕᒋᑦ ᓇᕿᓪᓚᕐᓯᐊᕆᔭᐅᓴᕐᓂᖕᒋᑦ ᐊᑐᖅᑕᐅᔪᓐᓇᕐᓂᖕᒋᑦ ᓴᖅᑭᖅᑐᖅ ᑕᕝᕙᓂ ᓴᐃᓐᓇᖅ ᐊᕕᑦᑐᖅᓯᒪᔪᒥ. ᐊᑯᓗ ᐊᔾᔨᙳᐊᖅ 1 ᓇᓗᓇᐃᔭᖅᓯᒪᓂᖕᒋᓐᓄᑦ.

Debris flow susceptibility maps were produced at a regional scale to best represent Grise Fiord. They identify potential source and propagation areas for debris flows. The entire analysis is based on a 6 m digital elevation model (DEM) and high-resolution satellite imagery. The debris flow susceptibility map was completed following the steps of Horton et al. (2013) using Flow-R.

The resulting susceptibility map for debris flows is illustrated in Figure 1. It shows the potential areas on steep slopes where debris flows can occur and how far they could travel, and are particularly focused on slopes with intense gullying or existing stream valleys. Many streams show a high potential for debris flow occurrence, and the modelling was very consistent with observations retrieved from satellite imagery (Figure 2). All of the existing debris flow deposits observed on satellite imagery correlate with a potential debris flow zone.

ᓴᓂᑦ ᐃᖏᕋᓂᖕᒋᑦ ᓇᕿᓪᓚᕐᓯᐊᕆᔭᐅᓴᕐᓂᖕᒋᑦ

ᓴᓂᑦ ᐃᖏᕋᓂᖕᒋᑦ ᓇᕿᓪᓚᕐᓯᐊᕆᔭᐅᓴᕐᓂᖕᒋᑦ ᓄᓇᙳᐊᑦ ᓴᖅᑭᖅᑎᑕᐅᓚᐅᖅᑐᑦ ᐊᕕᑦᑐᖅᓯᒪᔪᑦ ᐊᖏᓂᓪᓗ ᑭᒡᒐᖅᑐᐃᑎᐊᓛᖑᓗᑎ ᐊᐅᓱᐃᑦᑐᒥ. ᓇᓗᓇᐃᖅᓯᔪᑦ ᓇᕿᓪᓚᕐᓯᐊᕆᔭᐅᓴᕐᓂᖓᓂ ᐊᒻᒪ ᓯᐊᒻᒪᖅᐱᑦᑐᕐᓂᖓᓂ ᓴᓂᑦ ᐃᖏᕋᓂᖕᓄᑦ. ᐊᑦᑐᕐᒥᓪᓚᒍᑦ ᖃᐅᔨᓴᕐᓂᖅ ᑐᙵᓂᖃᖅᑐᖅ 2 ᒦᑕᐃᑦ ᖃᕋᓴᐅᔭᒃᑯᑦ ᖁᑦᑎᓐᓂᖓ ᐊᑐᖅᑕᐅᔪᓐᓇᖅᑐᑦ (DEM) ᐊᒻᒪ ᐊᔾᔨᙳᐊᑦᑎᐊᕙᐅᓂᖏᑦ ᖁᒻᒧᐊᑦᑎᑕᐅᓯᒪᔪᓂᑦ ᐊᔾᔨᙳᐊᓂᑦ. ᓴᓂᑦ ᐃᖏᕋᓂᖕᒋᑦ ᓇᕿᓪᓚᕐᓯᐊᕆᔭᐅᓴᕐᓂᖕᒋᓐᓂ ᓄᓇᙳᐊᖅ ᐱᔭᕇᖅᑕᐅᓚᐅᖅᑐᖅ ᒪᓕᑦᑐᒋ ᐊᑐᖅᑕᐅᓯᒪᓕᐊᓂᓐᓂᑦ ᕼᐅᐊᕐᑕᓐ ᐱᓕᕆᖃᑎᖏᓗ (2013) ᐊᑐᖅᑐᒋ Flow-R.

ᖃᐅᔨᓴᕐᓂᖕᒋᑦ ᓇᕿᓪᓚᕐᓯᐊᕆᔭᐅᓴᕐᓂᖕᒋᓐᓄᑦ ᓄᓇᙳᐊᖅ ᓴᓂᖕᓄᑦ ᐃᖏᕋᓂᖕᒋᓐᓄᑦ ᑕᑯᔅᓴᐅᑎᑕᐅᔪᖅ ᐊᔾᔨᙳᐊᖅ 1. ᓇᕿᓪᓚᕐᓯᐊᕆᔭᐅᓴᕐᓂᖕᒋᓐᓄᑦ ᓄᓇᙳᐊᖅ ᑕᑯᔅᓴᐅᑎᑦᑎᔪᑦ ᓯᕙᖕᒪᓂᖅᓴᓂᑦ ᓴᓂᑦ ᐃᖏᕋᓇᓪᓚᑦᑕᕐᒥᑦ ᐊᒻᒪ ᖃᓄᑎᒋ ᐅᖓᓯᒃᑎᒋᔪᓐᓇᕆᐊᖃᕐᓂᖓᓂ, ᐊᒻᒪ ᐱᑕᖃᓪᓚᕆᒃᑐᓂ ᓴᓂᑦ ᐃᖏᕋᓂᖕᒋᓐᓂ ᐸᖅᓯᔪᖃᖅᑕᐅᔪᒪᔪᒃ ᓇᖅᓴᖕᒋᑦᑎᐊᖅᑐᓂ ᐅᕙᓘᓂᑦ ᓇᖅᓴᓐᓂᑦ ᑭᒃᑲᓯᑎᑦᑎᖕᒪᓯᖕᒪᓃᑦᑐᓂ. ᐊᒥᓱᑦ ᑕᑯᔅᓴᐅᑎᑦᑎᔪᑦ ᖃᐅᔨᒪᓂᖅᑐᒥ ᐱᑦᑕᖕᒪᓃᑦᑐᓂ ᓴᓂᑦ ᐃᖏᕋᓂᖕᒋᓐᓂ, ᐊᒻᒪ ᒥᑦᓴᐅᓯᑕᐅᔪᑦ ᐊᔾᔨᖃᓪᓚᑕᐅᔪᑦ ᖃᐅᔨᓴᐅᑎᐅᔪᓂᑦ ᓴᖅᑭᑕᐅᔪᓂᑦ ᓴᓂᑦ ᐃᖏᕋᓂᖕᒋᓐᓂ ᑭᓪᓚᖕ.

Rock slope failure inventory

Figure 3. (left) Example of Advanced (orange) and Proven (yellow) landslides from the rock slope failure inventory results. Arrow points to a landslide deposit, outlined by the dashed line, supporting the inventory results that this slope is unstable. (right) Hillshade relief image of a digital elevation model of the same area.
ᐊᔾᔨᙳᐊᖅ 3. (ᓴᐅᒥᒥ) ᐆᑦᑑᑎᒋᓗᒍ ᓯᕗᓕᖅᑐᑦ (ᐊᐅᐸᓪᓚᖅᑐᖅ) ᒪᓕᑦᑕᖅᑲᓐᓂᖅᑐᑦ (ᖁᖅᓱᖅᑐᖅ) ᑎᓲᖅᑐᑦ ᐅᔭᖅᑲᐃᑦ ᓯᕗᓕᒧᓂ ᑎᓲᕐᓂᖏᓐᓂ ᑎᑎᖅᓯᒪᔪᑦ. ᖃᔾᔨᙳᐊᖅ ᑎᑯᐊᖕᒪᔪᑦ ᑎᓲᕐᓂᕐᒥᓄᑦ, ᑎᑎᖅᓯᒪᔪᑦ ᓯᓚᑖᒍᑦ, ᐃᑲᔪᖅᑐᐃᔪᑦ ᖃᐅᔨᓴᕐᓂᖕᒋᓐᓄᑦ ᑖᓐᓇ ᓯᕗᓕᖅᑐᖅ ᒪᑭᑕᓗᐊᖕᒋᒍᓐᓇᖅᑐᖅ. (ᑕᓕᖅᐱᒥ) ᓱᖃᓂᖅᐱᓂᖅᑲᒍ ᐊᔾᔨᙳᐊᖅ ᖃᕋᓴᐅᔭᒃᑯᑦ ᐊᑐᖅᑕᐅᔪᖅ ᖁᑦᑎᓐᓂᖓᓂ ᑕᕝᕙᓂ ᓇᒥᓐᓂᖕᒋᓐᓄᑦ.

An inventory of 55 rock slopes with signs of deformation were identified in the study area (Figure 1) and their runout areas modelled. The development stage expresses the level of certainty of the observations on the DEM and aerial imagery and is divided into four classes.

1) **Advanced**: the rock slope shows clear signs of postglacial deformation. This includes a clear opening of the back-scarp, but also the development of one or more other morphological criteria (flank development, open internal fractures, irregular morphology, depressions, graben, etc.)
2) **Proven**: where the rock face shows clear signs of postglacial deformation, includes a clear opening of the back scarp, while other morphological criteria are not present or are uncertain (flank development, open internal fractures, irregular morphology, depressions, graben, etc.).
3) **Potential**: the rock slope has a favorable structural arrangement to form an instability but shows no signs of postglacial deformation. However, rock avalanches have occurred in the immediate vicinity (with the same structural arrangement). This development stage also applies to rock slopes with uncertain signs of postglacial deformation. For example, if the opening of the back-scarp is uncertain but can be assumed or if the rock mass is highly fractured.
4) **Residual**: the rock slope has a favorable structural arrangement to form an instability but there is no evidence of postglacial deformation, past rock avalanches in the vicinity, or highly fractured rock mass

Two additional potential sackungs (large-scale, deep-seated gravitational slope deformation structures) that fell outside this classification scheme due to their large size and complexity were also documented. Finally, the runout area from these instabilities were also documented.

ᐅᔭᖅᑲᑦ ᓯᕗᓕᖅᑐᑦ ᑎᓲᕐᓂᖏᑦ

ᑎᑎᖅᑕᖅᓯᒪᔪᑦ 55 ᐅᔭᖅᑲᐃᑦ ᓯᕗᓕᖅᑐᑦ ᖃᐅᔨᓴᕐᓂᖕᒪᓕᒫᓂᖕᒋᓐᓄᑦ ᓇᓗᓇᐃᖅᑕᐅᓚᐅᖅᑐᑦ ᖃᐅᔨᓴᕐᕕᐅᔪᒥᑦ (ᐊᔾᔨᙳᐊᖅ 1). ᐱᕙᓪᓕᐊᓂᕆᔭᖓ ᓇᓗᓇᐃᖅᓯᔪᑦ ᖁᕝᕙᓯᓐᓂᖓ ᓇᓗᓇᖕᒋᑦᑐᒥ ᑕᑯᔭᐅᓂᖕᒋᓐᓄᑦ ᐅᖕᓇ DEM ᐊᒻᒪ ᖃᖓᑕᔫᒃᑯᑦ ᐊᔾᔨᙳᐊᓂ ᐊᒻᒪ ᐊᒻᒪᓗ ᐊᕕᑦᑐᖅᓯᒪᔪᑦ ᑎᓴᒪᓕᒫᓄᑦ ᖃᐅᔨᑦᑐᒐᑕᐅᓂᖕᒋᓐᓄᑦ.

1) **ᓯᕗᓪᓕᐅᑐᖅ**: ᐅᔭᖅᑲᐃᑦ ᓯᕗᓕᖕᒋᑦ ᑕᑯᔅᓴᐅᑎᑦᑎᓐᓂᐊᖅᑐᑦ ᐊᐅᓯᑦᑐᓚᐅᖅᑐᒍᑦ ᖃᐅᔨᓴᕐᓂᖕᓂᒃᓴᔭᖅᑦ. ᑖᓐᓇ ᐱᖃᓯᐅᔭᖅᓯᔪᖅ ᒪᑐᐃᖕᒪᓂᖅᑐᑦ ᑐᓄᐊᒍ, ᑭᓯᐊᓂ ᐱᕙᓪᓕᐊᓂᖕᒪ ᐊᑕᐅᓯᖅ ᐊᑕᐅᓯᕐᓗᐊᖅᑐᒍᑦ ᐊᓯᖕᒋᑦ ᐋᖅᑭᓯᒪᓂᖕᒋᑦ (ᖃᖕᒪᓪᓚᑎᑦᑎᔪᑦ, ᒪᑐᐃᖕᒪᔪᑦ ᐃᓗᐊᓃᑦᑐᑦ ᓄᖑᓯᒪᔪᑦ, ᐋᖅᑭᖅᓯᒪᙱᑦᑐᑦ, ᐃᓱᖃᖓᑦᑐᓂᖕᒋᑦ, ᐊᓯᖕᒋᑦ ᐊᓯᖏᓗ.)
2) **ᓇᓗᓇᐃᖅᑕᐅᓯᒪᔪᑦ**: ᐅᔭᖅᑲᐃᑦ ᑕᑯᔅᓴᐅᑎᑦᑎᓐᓂᖅᑐᖅ ᑭᖑᓪᓕᖓᓂ ᐊᐅᔭᐅᑎᓪᓗᒍ ᖃᐅᔨᓴᕐᓂᖕᓂᒃᓴᖅᑦ, ᐱᒃᓯᐅᒃᐅᔭᐅᑦ ᒪᑐᐃᖕᒪᓂᖅᑐᑦ ᑐᓄᐊᒍ, ᑭᓯᐊᓂ ᐊᓯᖕᒋᑦ ᐋᖅᑭᓯᒪᓂᖕᒋᑦ ᐋᖅᑭᓯᒪᓂᖕᒋᑦ ᐱᑕᖃᙱᖕᒋᑦᑐᑦ ᐅᕙᓘᓂᑦ ᓇᓗᓇᖅᑐᑦ (ᖃᖕᒪᓪᓚᑎᑦᑎᔪᑦ, ᒪᑐᐃᖕᒪᔪᑦ ᐃᓗᐊᓃᑦᑐᑦ ᓄᖑᓯᒪᔪᑦ, ᐋᖅᑭᖅᓯᒪᙱᑦᑐᑦ, ᐃᓱᖃᖓᑦᑐᓂᖕᒋᑦ, ᐊᓯᖕᒋᑦ ᐊᓯᖏᓗ.).
3) **ᐱᑕᖃᕈᓐᓇᖅᑐᖅ**: ᐅᔭᖅᑲᑦ ᓯᕗᓕᖕᒋᑦ ᐋᖅᑭᓯᒪᓂᖓ ᐊᑐᖅᑐᑦ ᐋᖅᑭᓯᒪᓪᓗᑎ ᒪᑭᑕᖃᕐᓂᖕᒋᑐᓂ ᑭᓯᐊᓂ ᐅᔭᖅᑲᐃᑦ ᑎᓲᖅᑕᖅᓯᒪᔪᑦ ᑕᕝᕙᓂ ᓯᕗᓕᖕᒋᑦ (ᐊᔾᔨᐅᖕᒋᖕᒋᑦ ᓴᓇᓯᒪᓂᖓ ᐋᖅᑭᓯᒪᓂᖕᒋᑦ). ᑖᓐᓇ ᐱᕙᓪᓕᐊᑎᑦᑎᓂᖓ ᓇᒻᒥᓂᖅ ᐊᑐᖅᑕᐅᓲᖅ ᐅᔭᖅᑲᑦ ᓯᕗᓕᖕᒋᑦ ᓄᓇᓕᐅᖅᑕᐅᔪᖅ ᐊᑐᖅᑕᐅᓂᖕᒋᓐᓄᑦ ᑎᓲᕐᓂᖅᑐᓂᑦ ᖃᐅᔨᓴᕐᓂᖕᓂᒃᓴᖅᑦ, ᐆᑦᑑᑎᒋᓗᒍ ᒪᑐᐃᖕᒪᓂᖓ ᑐᓄᐊᒍ ᓇᓗᓇᖅᐳᖅ ᑭᓯᐊᓂᓕ ᐃᓱᒪᒋᔭᐅᔪᓐᓇᖅᑐᖅ ᐅᕙᓘᓂᑦ ᐅᔭᖅᑲᐃᑦ ᐊᖕᒋᔪᑦ ᓄᖑᓯᒪᓪᓚᕆᒃᐸᑦ.
4) **ᐊᒥᐊᒃᑯᕐᓂᖕᒋᑦ**: ᐅᔭᖅᑲᐃᑦ ᓯᕗᓕᖕᒋᑦ ᐋᖅᑭᓯᒪᓂᖕᒋᓐᓄᑦ ᐊᑐᕈᓐᓇᖅᑐᑦ ᒪᑭᑕᖃᕐᓂᖕᒋᑐᓂ ᑭᓯᐊᓂᓕ ᖃᐅᔨᓴᖅᑕᐅᓯᒪᔪᑦ ᐊᑐᖅᑕᐅᔪᓐᓇᕐᓂᖕᒋᑦ ᑎᓲᕐᓂᖅᑐᓂᑦ, ᐅᔭᖅᑲᐃᑦ ᑎᓲᖅᑕᖅᓯᒪᓂᖅᑲᑎ, ᐅᕙᓘᓂᑦ ᐊᖕᒋᔪᑦ ᓄᖑᓯᒪᓪᓚᕆᒃᐸᑦ ᐅᔭᖅᑲᑦ ᐊᖕᒋᔪᑦ

ᒪᕐᕉᖕᓂᒃ ᐊᖕᒋᔪᑦ ᑎᓲᕐᓂᖃᕈᓐᓇᖅᑐᑦ (ᐊᖕᒋᔪᑦ, ᐃᑎᔪᒥ ᑲᑉᐸᖅᑐᓂᖓᓗ ᖃᐅᔨᓴᕐᓂᖅᑐᑦ ᓯᕗᓕᖅᑐᑦ) ᓯᓚᑖᓂᓪᓗᒋᑦ ᓇᓗᓇᐃᖅᑕᐅᓂᖕᒋᓐᓂ ᐊᖕᒋᓂᖏᓐᓄᑦ ᐱᔪᓐᓇᖅᑐᒥ ᐊᕙᑐᖅᑕᐅᓂᖕᒋᓐᓄᑦ ᐊᒻᒪ ᓇᓗᓇᖅᑐᓂᖕᒋᓐᓄᑦ ᑎᑎᖅᑕᐅᓯᒪᔪᑦ.

References

Normandeau A, Blais-Stevens A, Horton P, Oppikofer T, Sedore P, Maselli V. 2022. Landslides and debris flows in Pangnirtung Fiord, Nunavut; Geological Survey of Canada, Open File 8843, 1 poster. https://doi.org/10.4095/329219
Gosse JC, Tremblay T, Broom LA, Campbell DC, Wenzel G, Nedimovic MR, Brisson LF. 2020. Initial results from the ULINNIQ seismicity and tsunami hazard project, northeastern Baffin Island, Nunavut; in Summary of Activities 2019, Canada-Nunavut Geoscience Office, p. 101–124.
Higman B, Shugar DH, Stark CP, Ekström G, Koppes MN, Lynett P, Dufresne A, Haeussler PJ, Geertsema M, Gulick S, Mattox A, Venditti JG, Walton MAL, McCall N, Mckittrick E, MacInnes B, Bilderback EL, Tang H, Willis MJ, Richmond B, Reece RS, Larsen C, Olson B, Capra J, Ayca A, Bloom C, Williams H, Bonna D, Weiss R, Keen A, Skanavis V, Loso M. 2018. The 2015 landslide and tsunami in Taan Fiord, Alaska. Scientific Reports 9, 12993. https://doi.org/10.1038/s41598-018-30475-w
Horton P, Jaboyedoff M, Rudaz B, Zimmermann M. 2013. Flow-R, a model for susceptibility mapping of debris flows and other gravitational hazards at a regional scale;. Natural Hazards and Earth System Sciences, v. 13/4, p. 869-885. https://doi.org/10.5194/nhess-13-869-2013

[1]Geological Survey of Canada, 1 Challenger Drive, P.O. Box 1006, Dartmouth, Nova Scotia
[2]Terranum Sàrl, Rue de l'Industrie 35 bis, 1030 Bussigny, Switzerland
[3]Département de biologie, chimie et géographie, Université du Québec à Rimouski, 300, allée des Ursulines, Rimouski, Québec
[4]Geological Survey of Canada, 601 Booth Street, Ottawa, Ontario.

For more information, please contact J.B.R. Eamer (jordan.eamer@nrcan-rncan.gc.ca).

Permanent link: https://doi.org/10.4095/331096

This publication is available for free download through GEOSCAN (https://geoscan.nrcan.gc.ca/).

OPEN FILE
DOSSIER PUBLIC
8929
GEOLOGICAL SURVEY OF CANADA
COMMISSION GÉOLOGIQUE DU CANADA
2022

Publications in this series have not been edited; they are released as submitted by the author.
Les publications de cette série ne sont pas révisées; elles sont publiées telles que soumises par l'auteur.

ISSN 2816-7155
ISBN 978-0-660-46223-3
Catalogue No. M183-2/8929E-PDF

Recommended citation
Eamer, J.B.R., Normandeau, A., Horton, P., Oppikofer, T., Michoud, C., Didier, D., and Blais-Stevens, A., 2022. Landslides and debris flows in Grise Fiord, near Ausuittuq, Nunavut; Geological Survey of Canada, Open File 8929, 1 poster.
https://doi.org/10.4095/331096